JCAMECH

Vol. 47, No. 2, December 2016, pp 159-180
DOI: 10.22059/jcamech.2017.140165.97

Analysis of Euler-Bernoulli nanobeams: A mechanical-based solution

Mohammad Zakeri *, Reza Attarnejad, Amir Mohsen Ershadbakhsh

School of Civil Engineering, College of Engineering, University of Tehran, Tehran, Iran

Received: 10 Jan. 2016 , Accepted: 8 Nov. 2016

Abstract

The accuracy and efficiency of the elements proposed by finite element method (FEM) considerably depend on the interpolating functions namely shape functions used to formulate the displacement field within the element. In the present study, novel functions, namely basic displacements functions (BDFs), are introduced and exploited for structural analysis of nanobeams using finite element method based on Eringen's nonlocal elasticity and Euler-Bernoulli beam theory. BDFs are obtained through solving the governing differential equation of motion of nanobeams using the power series method. Unlike the conventional methods which are almost categorized as displacement-based methods, the flexibility basis of the method ensures true satisfaction of equilibrium equations at any interior point of the element. Accordingly, shape functions and structural matrices are achieved in terms of BDFs by application of merely mechanical principles. In order to evaluate the competency and accuracy of the proposed method with different boundary conditions, several numerical examples with various boundary conditions are scrutinized. Carrying out several numerical examples, the results in stability analysis, free longitudinal vibration and free transverse vibration show a complete accordance with those in literature.

Keywords: *Nanobeams, size-effect, Basic displacement functions (BDFs), Free vibration, Instability analysis*

1. Introduction

Due to rapidly developing nanotechnology industries, which lead to more advanced nano electromechanical equipment [1-3], the research in the field of mechanical properties of these nano-scale devices has attracted a great deal of attention. There are many researches in the literature substantiating that the mechanical characteristics of materials including elasticity modulus, flexural stiffness and etc. are greatly dependent on their size [4-7]. Basically, this effect is pertinent to atoms and molecules forming the material. The classical continuum theories aren't able to properly describe the structural behavior when dimensions of the structure become comparable to the nano-structural size of its material. Discrete models and modified continuum theories are the two common methods presented in order to take into account the size-dependent mechanical properties. Discrete models for instance molecular dynamics simulation are appropriate in precisely modeling nano-scale structures [8]. Among the modified continuum theories, the most frequent used in the literature are gradient elasticity theories, modified coupled theory and nonlocal elastic theories.

The nonlocal elasticity theory proposed by Eringen [9-12] is used by many researchers because of its competency based on which some of the shortcomings

* Corresponding Author. Tel.: +989127935898
Email Address: mohammad_zakeri@ut.ac.ir

Nomenclature

l Beam length

x Longitudinal coordinate

E Modulus of elasticity

E_0 Modulus of elasticity at origin

A Cross-sectional area

A_0 Cross-sectional area at origin

ρ Mass density

ρ_0 Mass density at origin

I Moment of inertia

I_0 Moment of inertia at origin

$w(x,t)$ Transverse displacement

$u(x,t)$ Axial displacement

NE Total number of beam elements

$q(x), n(x)$ External loading

$b_{u1}, b_{w1}, b_{\theta 1}, b_{u2}, b_{w2}, b_{\theta 2}$

Basic Displacement Functions

$\mathbf{b}'_w, \mathbf{b}''_w$ First and second derivative of $\mathbf{b}_w$ with respect to x

$\mathbf{b}'_u$ First derivative of $\mathbf{b}_u$ with respect to x

F_i Equivalent nodal forces

$\mathbf{F_{11}}$ Nodal flexibility matrix of the left node

$\mathbf{F}_{22}$ Nodal flexibility matrix of the right node

$\mathbf{G_a}$ Matrix containing nodal axial stiffness matrices

$\mathbf{G_f}$ Matrix containing nodal flexural stiffness matrices

$\mathbf{N_u}, \mathbf{N_w}$ Shape functions

$\mathbf{N}'_\mathbf{w}, \mathbf{N}''_\mathbf{w}$ First and second derivative of $\mathbf{N_w}$ with respect to x

$\mathbf{N}'_\mathbf{u}$ First derivative of $\mathbf{N_u}$ with respect to x

$\mathbf{K_g}$ Element geometrical stiffness matrix

$\mathbf{K_a}$ Element axial stiffness matrix

$\mathbf{K_f}$ Element flexural stiffness matrix

$\mathbf{M_a}$, $\mathbf{M_f}$ Element consistent mass matrix

α Non-dimensional size effect parameter

μ_L Non-dimensional longitudinal frequencies

μ_T Non-dimensional transverse natural frequencies

of the classical continuum theory can be completely obviated. Especially, it is useful in analysis of carbon nanotubes [13-14]. The nonlocal elasticity theory of Eringen is developed and formulated by many researchers [15-23]. These formulations can be categorized into differential nonlocal form [15-18] and integral nonlocal form [19-23]. The distinctive differences between integral and differential forms are described by Lim [20]. Among the nonlocal elasticity theories, nonlocal differential elasticity is the most commonly used in the analysis of nano-scaled structures because of its simplicity [19].

Wang & Wang [24] presented the constitutive relations of nonlocal elasticity theory for application in the analysis of carbon nanotubes (CNTs) when modelled as Euler–Bernoulli beams, Timoshenko beams or as cylindrical shells.

The small scale effect on the axial vibration of a tapered nanorod was studied by Danesh et al. using nonlocal elasticity theory and DQM method. It was concluded that the nonlocal effect has a significant influence on the axial vibration of nanorods [25]. Moreover, Aghababaei and Reddy [26] presented a third-order shear deformation plate theory capable of capturing both small scale effects and shear stress

through the plate thickness and clarifed the effect of nonlocal theory on natural vibration frequency of the plates. Furthermore, the buckling behavior of nanoscale circular plates under uniform radial compression was scrutinized by Farajpour et al. [27] to evaluate and illustrate the small-scale effect in the buckling of circular nanoplates.

The application of thin beams in nano-scale devices such as Nano-Electro-Mechanical Systems (MEMS), atomic force microscopes and etc. in which small-scale size effects are commonly observed [28], has gained considerable attention in the literature. Euler-Bernoulli beam theory based on Eringen's nonlocal elasticity theory is an innovative solution presented for the analysis of thin beams in nano-scale applications [29].

Nonlocal Euler-Bernoulli beam theory was implemented by Peddieson et al. to investigate the flexural behavior of a nano beam based on which the importance of nonlocal effects was estimated [13]. Xu [30] employed the integral equation approach and the nonlocal elasticity theory to scrutinize the nonlocal effect on the free transverse vibrations of nano-to-micron scale beams and demonstrated a noticeable influence on higher vibration modes.

Reddy [31], analytically examined bending, buckling and vibration of nanobeams through reformulating various local beam theories by means of the nonlocal differential constitutive relations of Eringen. Wang et al. [32] obtained governing equations and boundary conditions for the free vibration of beams in accordance with Timoshenko beam theory and Eringen's nonlocal elasticity theory.

Heireche et al. [33] modeled a single-elastic beam based on the Bernoulli–Euler and Timoshenko beam theories using nonlocal elasticity for the wave propagation in carbon nanotubes (CNTs). Furthermore, Aydogu [34] suggested a generalized nonlocal beam theory whose formulation is based on nonlocal constitutive equations of Eringen, to examine bending, buckling, and free vibration of nanobeams.

Kong et al. [35] formulated free vibration of Euler–Bernoulli micro-beams based on modified couple stress theory. Additionally, the static and dynamic problems of Euler–Bernoulli beams are analytically solved according to strain gradient elasticity theory by Kong et al. [36]. Filiz and Aydogu [37] investigated vibration of carbon nanotube heterojunctions along axial direction implementing nonlocal rod theory in which the nonlocal constitutive equations of Eringen are used.

In addition, finite element formulations for analysis of Euler–Bernoulli nanobeam and Kirchoff nanoplate have been presented by Phadikar and Pradhan [19] which are based on nonlocal differential elasticity theory. Finite element results for bending, buckling and vibration for nonlocal beam are obtained. Xia et al. [38] implemented DQM to study static and dynamic behavior of nonlinear microbeams. The presented nonlinear model is conducted within the context of non-classical continuum mechanics by defining a material length scale parameter. Wang et al. [39] modeled a buckling of nanotubes embedded in an elastic matrix on the basis of Timoshenko beam theory. Both of stress gradient and strain gradient approaches are followed.

In order to investigate the small-scale effect on the axial vibration of nano-rods, Aydogdu developed a nonlocal elastic rod model and obtained explicit expressions for natural frequencies of the rod with different boundary conditions [40]. Moreover, Wang et al. [41] investigated the elastic buckling analysis of micro- and nano-rods/tubes according to the nonlocal elasticity theory of Eringen. They proposed explicit expressions for calculating the critical buckling loads of axially loaded rods/tubes with various boundary conditions.

In an attempt to solve the governing differential equation of non-prismatic beams, Attarnejad [42] introduced the novel concept of BDFs. Subsequently, Attarnejad and Shahba extended the scope for both of static [42-45] and dynamic [46-49] BDFs which are used in different beam theories. In this paper, we aim to propose a new application of dynamic BDFs for nanobeams. Firstly, BDFs are briefly described and calculated through a power series solution for governing differential equation of Euler-Bernoulli nanobeams. Afterwards, shape functions and structural matrices are derived in term of BDFs based on the analysis procedure is carried out. In order to evaluate the efficiency and competency of the proposed method several numerical examples are presented and the results show a good agreement with those in literature.

2. Basic Displacement Functions

BDFs are apparently mathematical functions holding a profound mechanical concept. In the following section, firstly, the explicit definitions of BDFs and the calculation procedure are described. Accordingly, nodal flexibility matrices of the system are developed based on the BDFs.

BDFs definition:

b_{w1}: Transverse displacement of the left node due to a unit lateral load at distance x when the beam is free-clamped as depicted in Figure 1(a).

$b_{\theta 1}$: Angle of rotation of the left node due to a unit lateral load at distance x when the beam is free-clamped as depicted in Figure 1(b).

b_{w2}: Transverse displacement of the right node due to a unit lateral load at distance x when the beam is clamped-free as depicted in Figure 1(c).

$b_{\theta 2}$: Angle of rotation of the right node due to a unit lateral load at distance x when the beam is clamped-free as depicted in Figure 1(d).

b_{u1}: Axial displacement of the left node due to a unit axial load at distance x when the beam is free-clamped as depicted in Figure 1(e).

b_{u2}: Axial displacement of the right node due to a unit axial load at distance x when the beam is clamped-free as depicted in Figure 1(f).

Regarding the well-known reciprocal theorem, BDFs can be redefined through the following procedure:

b_{w1}: Transverse displacement at distance x due to a unit lateral load at the left node of the free-clamped beam as shown in Figure 2(a).

$b_{\theta 1}$: Transverse displacement at distance x due to a unit moment at the left node of a free-clamped beam as shown in Figure 2(b).

b_{w2}: Transverse displacement at distance x due to a unit lateral load at the right node of a clamped-free beam as shown in Figure 2(c).

$b_{\theta 2}$: Transverse displacement at distance x due to a unit moment at the right node of a clamped-free beam as shown in Figure 2(d).

b_{u1}: Axial displacement at distance x due to a unit axial load at the left node of a free-clamped beam as shown in Figure 2(e).

b_{u2}: Axial displacement at distance x due to a unit axial load at the right node of a clamped-free beam as shown in Figure 2(f).

3. Calculating the BDFs:

Based on the equivalent definitions of BDFs As illustrated in Figure 2, BDFs can be expressed as the transverse and axial displacements of a cantilever beam at distance x due to a unit nodal load or moment depending on the type of BDF; thus, each BDF can be achieved through solving the governing differential equations in terms of transverse and axial displacements and imposing the corresponding boundary conditions. The governing differential

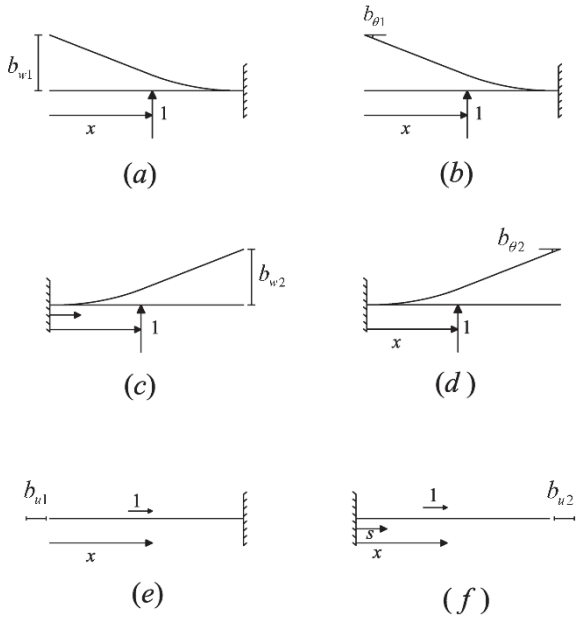

Figure 1. Description of BDFs: (a) b_{w1}; (b) $b_{\theta 1}$; (c) b_{w2}; (d) $b_{\theta 2}$; (e) b_{u1}; (f) b_{u2}

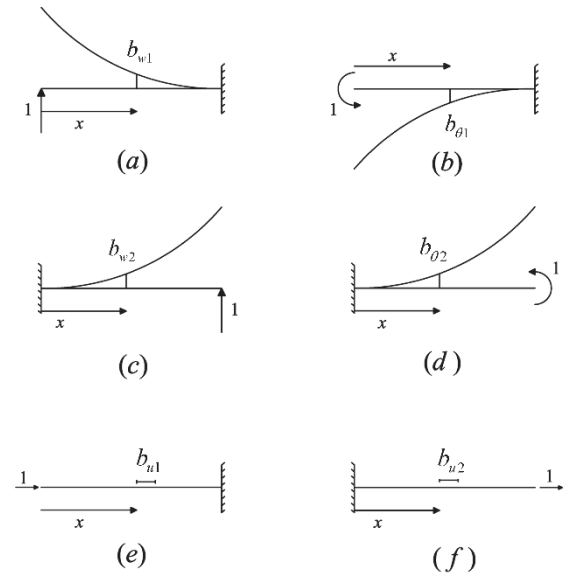

Figure 2. Equivalent definitions of BDFs: (a) b_{w1}; (b) $b_{\theta 1}$; (c) b_{w2}; (d) $b_{\theta 2}$; (e) b_{u1}; (f) b_{u2}

equations for the Euler-Bernoulli nano-beam are as follows [31]

$$\frac{\partial}{\partial x}\left(EA(x)\frac{\partial u}{\partial x}\right)+n(x,t)+\mu\left(\rho A(x)\frac{\partial^4 u}{\partial x^2\partial t^2}-\frac{\partial^2 n(x,t)}{\partial x^2}\right)-\rho A(x)\frac{\partial^2 u}{\partial t^2}=0 \quad (1a)$$

$$\frac{\partial^2}{\partial x^2}\left(EI(x)\frac{\partial^2 w}{\partial x^2}\right)-\mu\frac{\partial^2}{\partial x^2}\left(N\frac{\partial^2 w}{\partial x^2}-q(x,t)+\rho A(x)\frac{\partial^2 w}{\partial t^2}-\rho I(x)\frac{\partial^4 w}{\partial x^2\partial t^2}\right)$$
$$+N\frac{\partial^2 w}{\partial x^2}-q(x,t)+\rho A\frac{\partial^2 w}{\partial t^2}-\rho I\frac{\partial^4 w}{\partial x^2\partial t^2}=0 \quad (1b)$$

where $EI(x)$ and $EA(x)$ are flexural and axial stiffness respectively; $q(x,t)$ is the external lateral loading and $n(x,t)$ is the external axial loading. The parameter μ is defined as $\mu=(e_0a)^2$ in which e_0a captures the small scale effect on the response of the structure. N is a constant axial force within the element length.

Since all external forces in BDFs are point forces, $n(x,t)$ and $q(x,t)$ is set to zero. Moreover, the variation of axial and transverse displacements are assumed to be sinusoidal with a circular frequency of ω_L and ω_T respectively.

$$u(x,t)=U(x)\sin(\omega_L t) \quad (2a)$$
$$w(x,t)=W(x)\sin(\omega_T t) \quad (2b)$$

Then equations (1a) and (1b) are rewritten as

$$\frac{d}{dx}\left(EA(x)\frac{dU}{dx}\right)-\mu\left(\omega_L{}^2\rho A(x)\frac{d^2U}{dx^2}\right)+\omega_L{}^2\rho A(x)U=0 \quad (3a)$$

$$\frac{d^2}{dx^2}\left(EI(x)\frac{d^2W}{dx^2}\right)-\mu\frac{d^2}{dx^2}\left(N\frac{d^2W}{dx^2}-\omega_T{}^2\rho A(x)W+\omega_T{}^2\rho I(x)\frac{d^2W}{dx^2}\right)$$
$$+N\frac{d^2W}{dx^2}-\omega_T{}^2\rho AW+\omega_T^2\rho I\frac{d^2W}{dx^2}=0 \quad (3b)$$

Furthermore, introducing the dimensionless parameter $\xi=x/L$, equations (3a) and (3b) yield

$$EA(\xi)U''+EA'(\xi)U'-\omega_L{}^2\mu\rho A(\xi)U''+L^2\omega_L{}^2\rho A(\xi)U=0 \quad (4a)$$

$$EI(\xi)W^{(4)}+2EI'(\xi)W'''+EI''(\xi)W''-\mu NW^{(4)}+L^2\omega_T{}^2\mu\rho AW''+2L^2\omega_T{}^2\mu\rho A'W'$$
$$+L^2\omega_T{}^2\mu\rho A''W-\omega_T{}^2\mu\rho I''W''-2\omega_T{}^2\mu\rho I'W'''-\omega_T{}^2\mu\rho IW^{(4)}+L^2NW''$$
$$-L^4\omega_T{}^2\rho AW+L^2\omega_T{}^2\rho IW''=0 \quad (4b)$$

in which primes denote differentiation with respect to ξ.

The variations of both axial and flexural stiffness along the element can be defined in the form of power series respectively as [50-52]

$$EA(\xi)=\sum_{i=0}^{\infty}EA_i\xi^i \quad (5a)$$

$$EI(\xi)=\sum_{i=0}^{\infty}EI_i\xi^i \quad (5b)$$

The mass inertias ρA and ρI are represented in power series by

$$\rho A(\xi) = \sum_{i=0}^{\infty} \rho A_i \xi^i \tag{5c}$$

$$\rho I(\xi) = \sum_{i=0}^{\infty} \rho I_i \xi^i \tag{5d}$$

General solution of equations (4a) and (4b) can be represented by power series of the form

$$U(\xi) = \sum_{i=0}^{\infty} U_i \xi^i \tag{5e}$$

$$W(\xi) = \sum_{i=0}^{\infty} W_i \xi^i \tag{5f}$$

Consequently

$$U'(\xi) = \sum_{i=0}^{\infty} (i+1) U_{i+1} \xi^i \tag{5g}$$

$$U''(\xi) = \sum_{i=0}^{\infty} (i+1)(i+2) U_{i+2} \xi^i \tag{5h}$$

$$W'(\xi) = \sum_{i=0}^{\infty} (i+1) W_{i+1} \xi^i \tag{5i}$$

$$W''(\xi) = \sum_{i=0}^{\infty} (i+1)(i+2) W_{i+2} \xi^i \tag{5j}$$

$$W'''(\xi) = \sum_{i=0}^{\infty} (i+1)(i+2)(i+3) W_{i+3} \xi^i \tag{5k}$$

$$W^{(4)}(\xi) = \sum_{i=0}^{\infty} (i+1)(i+2)(i+3)(i+4) W_{i+4} \xi^i \tag{5l}$$

Substituting equations (5) into the every single term of equations (4) leads to

$$\begin{aligned} EAU''(\xi) &= \left[\left(\sum_{i=0}^{\infty} EA_i \xi^i \right) \left(\sum_{i=0}^{\infty} (i+1)(i+2) U_{i+2} \xi^i \right) \right] \\ &= \sum_{i=0}^{\infty} \left\{ \sum_{j=0}^{i} (j+1)(j+2) EA_{i-j} U_{j+2} \right\} \xi^i \end{aligned} \tag{6a}$$

$$EA'U'(\xi)=\left[\left(\sum_{i=0}^{\infty}(i+1)EA_{i+1}\xi^i\right)\left(\sum_{i=0}^{\infty}(i+1)U_{i+1}\xi^i\right)\right]$$
$$=\sum_{i=0}^{\infty}\left\{\sum_{j=0}^{i}(j+1)(i-j+1)EA_{i-j+1}U_{j+1}\right\}\xi^i \tag{6b}$$

$$\rho AU''(\xi)=\left[\left(\sum_{i=0}^{\infty}\rho A_i\xi^i\right)\left(\sum_{i=0}^{\infty}(i+1)(i+2)U_{i+2}\xi^i\right)\right]$$
$$=\sum_{i=0}^{\infty}\left\{\sum_{j=0}^{i}(j+1)(j+2)\rho A_{i-j}U_{j+2}\right\}\xi^i \tag{6c}$$

$$\rho A(\xi)U(\xi)=\left[\left(\sum_{i=0}^{\infty}\rho A_i\xi^i\right)\left(\sum_{i=0}^{\infty}U_i\xi^i\right)\right]=\sum_{i=0}^{\infty}\left\{\sum_{j=0}^{\infty}\left(\rho A_{i-j}U_j\right)\right\}\xi^i \tag{6d}$$

$$EI(\xi)W^{(4)}(\xi)=\left[\left(\sum_{i=0}^{\infty}EI_i\xi^i\right)\left(\sum_{i=0}^{\infty}(i+1)(i+2)(i+3)(i+4)W_{i+4}\xi^i\right)\right]$$
$$=\sum_{i=0}^{\infty}\left\{\sum_{j=0}^{i}(j+1)(j+2)(j+3)(j+4)EI_{i-j}W_{j+4}\right\}\xi^i \tag{6e}$$

$$EI'(\xi)W'''(\xi)=\left[\left(\sum_{i=0}^{\infty}(i+1)EI_{i+1}\xi^i\right)\left(\sum_{i=0}^{\infty}(i+1)(i+2)(i+3)W_{i+3}\xi^i\right)\right]$$
$$=\sum_{i=0}^{\infty}\left\{\sum_{j=0}^{i}(j+1)(j+2)(j+3)(i-j+1)EI_{i-j+1}W_{j+3}\right\}\xi^i \tag{6f}$$

$$EI''(\xi)W''(\xi)=\left[\left(\sum_{i=0}^{\infty}(i+1)(i+2)EI_{i+2}\xi^i\right)\left(\sum_{i=0}^{\infty}(i+1)(i+2)W_{i+2}\xi^i\right)\right]$$
$$=\sum_{i=0}^{\infty}\left\{\sum_{j=0}^{i}(j+1)(j+2)(i-j+1)(i-j+2)EI_{i-j+2}W_{j+2}\right\}\xi^i \tag{6g}$$

$$\rho A(\xi)W''(\xi)=\left[\left(\sum_{i=0}^{\infty}\rho A_i\xi^i\right)\left(\sum_{i=0}^{\infty}(i+1)(i+2)W_{i+2}\xi^i\right)\right]=\sum_{i=0}^{\infty}\left\{\sum_{j=0}^{\infty}(j+1)(j+2)\rho A_{i-j}W_{j+2}\right\}\xi^i \tag{6h}$$

$$\rho A'(\xi)W'(\xi)=\left[\left(\sum_{i=0}^{\infty}(i+1)\rho A_{i+1}\xi^i\right)\left(\sum_{i=0}^{\infty}(i+1)W_{i+1}\xi^i\right)\right]=\sum_{i=0}^{\infty}\left\{\sum_{j=0}^{\infty}(j+1)(i-j+1)\rho A_{i-j+1}W_{j+1}\right\}\xi^i \tag{6i}$$

$$\rho A''(\xi)W(\xi)=\left[\left(\sum_{i=0}^{\infty}(i+1)(i+2)\rho A_{i+2}\xi^i\right)\left(\sum_{i=0}^{\infty}W_i\xi^i\right)\right]=\sum_{i=0}^{\infty}\left\{\sum_{j=0}^{\infty}(i-j+1)(i-j+2)\rho A_{i-j+2}W_j\right\}\xi^i \tag{6j}$$

$$\rho A(\xi)W(\xi)=\left[\left(\sum_{i=0}^{\infty}\rho A_i\xi^i\right)\left(\sum_{i=0}^{\infty}W_i\xi^i\right)\right]=\sum_{i=0}^{\infty}\left\{\sum_{j=0}^{\infty}\left(\rho A_{i-j}W_j\right)\right\}\xi^i \tag{6k}$$

$$N(\xi)W''(\xi)=\left[\left(\sum_{i=0}^{\infty}N_i\xi^i\right)\left(\sum_{i=0}^{\infty}(i+1)(i+2)W_{i+2}\xi^i\right)\right]=\sum_{i=0}^{\infty}\left\{\sum_{j=0}^{\infty}(j+1)(j+2)N_{i-j}W_{j+2}\right\}\xi^i \tag{6m}$$

$$\begin{aligned}N(\xi)W^{(4)}(\xi)&=\left[\left(\sum_{i=0}^{\infty}N_i\xi^i\right)\left(\sum_{i=0}^{\infty}(i+1)(i+2)(i+3)(i+4)\right)W_{i+4}\xi^i\right]\\&=\sum_{i=0}^{\infty}\left\{\sum_{j=0}^{i}(j+1)(j+2)(j+3)(j+4)N_{i-j}W_{j+4}\right\}\xi^i\end{aligned} \tag{6n}$$

$$\begin{aligned}\rho I(\xi)W^{(4)}(\xi)&=\left[\left(\sum_{i=0}^{\infty}\rho I_i\xi^i\right)\left(\sum_{i=0}^{\infty}(i+1)(i+2)(i+3)(i+4)W_{i+4}\xi^i\right)\right]\\&=\sum_{i=0}^{\infty}\left\{\sum_{j=0}^{i}(j+1)(j+2)(j+3)(j+4)\rho I_{i-j}W_{j+4}\right\}\xi^i\end{aligned} \tag{6o}$$

$$\begin{aligned}\rho I'(\xi)W'''(\xi)&=\left[\left(\sum_{i=0}^{\infty}(i+1)\rho I_{i+1}\xi^i\right)\left(\sum_{i=0}^{\infty}(i+1)(i+2)(i+3)W_{i+3}\xi^i\right)\right]\\&=\sum_{i=0}^{\infty}\left\{\sum_{j=0}^{i}(j+1)(j+2)(j+3)(i-j+1)\rho I_{i-j+1}W_{j+3}\right\}\xi^i\end{aligned} \tag{6p}$$

$$\begin{aligned}\rho I''(\xi)W''(\xi)&=\left[\left(\sum_{i=0}^{\infty}(i+1)(i+2)\rho I_{i+2}\xi^i\right)\left(\sum_{i=0}^{\infty}(i+1)(i+2)W_{i+2}\xi^i\right)\right]\\&=\sum_{i=0}^{\infty}\left\{\sum_{j=0}^{i}(j+1)(j+2)(i-j+1)(i-j+2)\rho I_{i-j+2}W_{j+2}\right\}\xi^i\end{aligned} \tag{6q}$$

$$\rho I(\xi)W''(\xi)=\left[\left(\sum_{i=0}^{\infty}\rho I_i\xi^i\right)\left(\sum_{i=0}^{\infty}(i+1)(i+2)W_{i+2}\xi^i\right)\right]=\sum_{i=0}^{\infty}\left\{\sum_{j=0}^{\infty}(j+1)(j+2)\rho I_{i-j}W_{j+2}\right\}\xi^i \tag{6r}$$

Assembling equations (6) and equations (4) could be finally written as

$$\begin{aligned}\sum_{i=0}^{\infty}\Bigg\{&\sum_{j=0}^{i}(j+1)(j+2)EA_{i-j}U_{j+2}+\sum_{j=0}^{i}(j+1)(i-j+1)EA_{i-j+1}U_{j+1}\\&-\omega_L^2\mu\sum_{j=0}^{i}(j+1)(j+2)\rho A_{i-j}U_{j+2}+L^2\omega_L^2\sum_{j=0}^{i}\rho A_{i-j}U_j\Bigg\}\xi^i=0\end{aligned} \tag{7a}$$

$$\sum_{i=0}^{\infty}\Bigg\{\sum_{j=0}^{i}(j+1)(j+2)(j+3)(j+4)EI_{i-j}W_{j+4}+2\sum_{j=0}^{i}(j+1)(j+2)(j+3)(i-j+1)EI_{i-j+1}W_{j+3}$$
$$+\sum_{j=0}^{i}(j+1)(j+2)(i-j+1)(i-j+2)EI_{i-j+2}W_{j+2}-\sum_{j=0}^{i}(j+1)(j+2)(j+3)(j+4)\mu N_{i-j}W_{j+4}$$
$$+L^2\omega_T^2\mu\sum_{j=0}^{i}(j+1)(j+2)\rho A_{i-j}W_{j+2}+2L^2\omega_T^2\mu\sum_{j=0}^{i}(j+1)(i-j+1)\rho A_{i-j+1}W_{j+1}$$
$$+L^2\omega_T^2\mu\sum_{j=0}^{i}(i-j+1)(i-j+2)\rho A_{i-j+2}W_j-\omega_T^2\mu\sum_{j=0}^{i}(j+1)(j+2)(j+3)(j+4)\rho I_{i-j}W_{j+4} \qquad (7b)$$
$$-2\omega_T^2\mu\sum_{j=0}^{i}(j+1)(j+2)(j+3)(i-j+1)\rho I_{i-j+1}W_{j+3}-L^4\omega_T^2\sum_{j=0}^{i}\rho A_{i-j}W_j$$
$$-\omega_T^2\mu\sum_{j=0}^{i}(j+1)(j+2)(i-j+1)(i-j+2)\rho I_{i-j+2}W_{j+2}+L^2\sum_{j=0}^{i}(j+1)(j+2)N_{i-j}W_{j+2}$$
$$+L^2\omega_T^2\sum_{j=0}^{i}(j+1)(j+2)\rho I_{i-j}W_{j+2}\Bigg\}\xi^i=0$$

Satisfying equations (7a) and (7b) for all values of ξ,

recurrence formulas for U_i and W_i are achieved as

$$U_{i+2}=\frac{1}{(i+1)(i+2)\left(EA_0-\mu\omega_L^2\rho A_0\right)}\Bigg[-\sum_{j=0}^{i}(j+1)(i-j+1)\rho A_{i-j+1}U_{j+1}-L^2\sum_{j=0}^{i}\rho A_{i-j}U_j$$
$$-\sum_{j=0}^{i-1}(j+1)(j+2)\left\{EA_{i-j}-\mu\omega_L^2\rho A_{i-j}\right\}U_{j+2}\Bigg] \qquad (8a)$$

$$W_{i+4}=\frac{1}{(i+1)(i+2)(i+3)(i+4)\left(EI_0-\mu N-\mu\omega_T^2\rho I_0\right)}\Bigg[\sum_{j=0}^{i}L^4\omega_T^2\rho A_{i-j}W_j$$
$$-L^2\omega_T^2\mu\sum_{j=0}^{i}(j+1)(j+2)\rho A_{i-j}W_{j+2}+2(j+1)(i-j+1)\rho A_{i-j+1}W_{j+1}+(i-j+1)(i-j+2)\rho A_{i-j+2}W_j$$
$$-\sum_{j=0}^{i}\left\{(j+1)(j+2)(i-j+1)(i-j+2)EI_{i-j+2}W_{j+2}+2(j+1)(j+2)(j+3)(i-j+1)EI_{i-j+1}W_{j+3}\right\}$$
$$+\omega_T^2\mu\sum_{j=0}^{i}\left\{(j+1)(j+2)(i-j+1)(i-j+2)\rho I_{i-j+2}W_{j+2}+2(j+1)(j+2)(j+3)(i-j+1)\rho I_{i-j+1}W_{j+3}\right\}$$
$$-\sum_{j=0}^{i-1}(j+1)(j+2)(j+3)(j+4)(EI_{i-j}-\mu N_{i-j}-\mu\omega_T^2\rho I_{i-j})W_{j+4}$$
$$-L^2\sum_{j=0}^{i}(j+1)(j+2)N_{i-j}W_{j+2}+\omega_T^2(j+1)(j+2)\rho I_{i-j}W_{j+2}\Bigg]$$

$$for\ i=0,1,2,\ldots \qquad (8b)$$

Regarding the recurrence formulas, an explicit expression for longitudinal displacement $U(\xi)$ can be obtained in terms of the first two terms namely U_0 and U_1 as

$$U(\xi)=\begin{bmatrix}a_1(\xi) & a_2(\xi)\end{bmatrix}\begin{Bmatrix}U_0\\U_1\end{Bmatrix}=\mathbf{a}.\mathbf{U} \tag{9}$$

where a_i $(i=1,2)$ are polynomials resulted from solving equation (8a).

Similarly, transverse displacement $W(\xi)$ can be expressed in terms of four constants W_0, W_1, W_2 and W_3 as

$$W(\xi)=\begin{bmatrix}f_1(\xi) & f_2(\xi) & f_3(\xi) & f_4(\xi)\end{bmatrix}\begin{Bmatrix}W_0\\W_1\\W_2\\W_3\end{Bmatrix}=\mathbf{f}.\mathbf{W} \tag{10}$$

in which f_i $(i=1,2,3,4)$ are polynomial solutions of equation (8b) and $\mathbf{W}$ can be evaluated for each BDF through imposing the correspondent boundary conditions. As depicted in Figure 2, the boundary conditions for each BDF are

b_{w1}:

$$V\big|_{\xi=0}=1 \quad M\big|_{\xi=0}=0 \quad W\big|_{\xi=1}=0 \quad \theta\big|_{\xi=1}=0 \tag{11a}$$

$b_{\theta 1}$:

$$V\big|_{\xi=0}=0 \quad M\big|_{\xi=0}=-1 \quad W\big|_{\xi=1}=0 \quad \theta\big|_{\xi=1}=0 \tag{11b}$$

b_{w2}:

$$W\big|_{\xi=0}=0 \quad \theta\big|_{\xi=0}=0 \quad V\big|_{\xi=1}=-1 \quad M\big|_{\xi=1}=0 \tag{11c}$$

$b_{\theta 2}$:

$$W\big|_{\xi=0}=0 \quad \theta\big|_{\xi=0}=0 \quad V\big|_{\xi=1}=0 \quad M\big|_{\xi=1}=1 \tag{11d}$$

Additionally, the rotation angle, bending moments and shear forces are respectively expressed as [31]

$$N(\xi)=\frac{1}{L}EA\frac{\partial u}{\partial \xi}+\frac{1}{L}\mu\rho A\frac{\partial^3 u}{\partial \xi \partial t^2} \tag{12a}$$

$$\theta(\xi)=\frac{1}{L}\frac{\partial W}{\partial \xi} \tag{12b}$$

$$M(\xi)=-\frac{1}{L^2}\left[EI(\xi)\frac{\partial^2 w}{\partial \xi^2}\right]+\mu\left[N\frac{1}{L^2}\frac{\partial^2 w}{\partial \xi^2}+\rho A\frac{\partial^2 w}{\partial t^2}-\frac{1}{L^2}\rho I\frac{\partial^4 w}{\partial \xi^2 \partial t^2}\right] \tag{12c}$$

$$\begin{aligned}V(\xi)=&-\frac{1}{L^3}\left[\frac{\partial}{\partial \xi}\left(EI(\xi)\frac{\partial^2 w}{\partial x^2}\right)\right]-\frac{1}{L}N\frac{\partial w}{\partial \xi}\\&+\mu\frac{\partial}{\partial x}\left[\frac{1}{L^2}N\frac{\partial^2 w}{\partial \xi^2}+\rho A\frac{\partial^2 w}{\partial t^2}-\frac{1}{L^2}\rho I\frac{\partial^4 w}{\partial \xi^2 \partial t^2}\right]+\frac{1}{L}\rho I\frac{\partial^3 w}{\partial \xi \partial t^2}\end{aligned} \tag{12d}$$

Since BDFs are calculated through a static analysis, the time derivative terms should be ignored. Imposing the boundary conditions for each BDF results in a set of four simultaneous equations from which $\mathbf{W}$ is calculated.

b_{u1}:

$$N\big|_{\xi=0}=1 \quad U_{\xi=1}=0\ , \tag{13a}$$

b_{u2}:

$$U_{\xi=0}=0 \quad N\big|_{\xi=1}=1, \tag{13b}$$

4. New shape functions

Consider a general nanobeam with clamped-clamped boundary conditions. The element is subjected to distributed axial and lateral external loadings as illustrated in Figure 3(a). With the aim of calculating the support reactions, the structural system should be decomposed into statically determinate systems. Therefore, each cantilever beam as shown in Figure 3, is analyzed separately and finally the support reactions are obtained by applying the superposition principle.

$$\begin{Bmatrix} u_2 \\ w_2 \\ \theta_2 \end{Bmatrix}^{(b)} = \int_0^l n(x) \begin{Bmatrix} b_{u2} \\ 0 \\ 0 \end{Bmatrix} dx + \int_0^l q(x) \begin{Bmatrix} 0 \\ b_{w2} \\ b_{\theta 2} \end{Bmatrix} dx \tag{14}$$

where u_2, w_2 and θ_2 are the axial, lateral and rotational displacements at point (2) respectively. The

$$\begin{Bmatrix} u_2 \\ w_2 \\ \theta_2 \end{Bmatrix}^{(c)} = \mathbf{F_{22}} \begin{Bmatrix} N_2 \\ V_2 \\ M_2 \end{Bmatrix} \tag{15}$$

in which N_2, V_2 and M_2 are the axial force, shear force and bending moment at point (2) respectively.

$$\begin{Bmatrix} u_2 \\ w_2 \\ \theta_2 \end{Bmatrix}^{(b)} + \begin{Bmatrix} u_2 \\ w_2 \\ \theta_2 \end{Bmatrix}^{(c)} = \begin{Bmatrix} u_2 \\ w_2 \\ \theta_2 \end{Bmatrix}^{(a)} = \mathbf{0} \tag{16}$$

Substituting equations (14) and (15) into equation (16),

reaction forces are obtained as

$$\begin{Bmatrix} N_2 \\ V_2 \\ M_2 \end{Bmatrix} = -\mathbf{K_{22}} \left(\int_0^l n(x) \begin{Bmatrix} b_{u2} \\ 0 \\ 0 \end{Bmatrix} dx + \int_0^l q(x) \begin{Bmatrix} 0 \\ b_{w2} \\ b_{\theta 2} \end{Bmatrix} dx \right) \tag{17}$$

Following the similar procedure $\mathbf{U}$ could be evaluated for each BDF by imposing the appropriate boundary conditions. According to Figure 2, the boundary conditions for each BDF are as follows

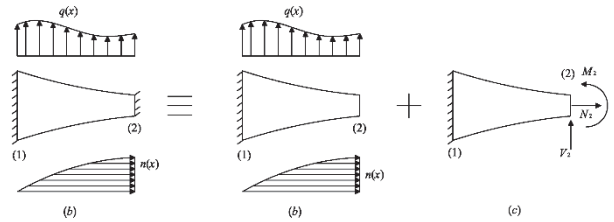

Figure 3. General beam element decomposed into isostatic structures.

Regarding the definitions of BDFs shown in Figure 1, one could express the nodal displacements of point (2) in Figure 3(b) in terms of BDFs as

nodal displacements of point (2) in Figure 3(c) can be obtained using flexibility matrix of point (2).

According to the superposition principle, one can easily write.

Following similar procedure for point (1) yields.

$$\begin{Bmatrix} N_1 \\ V_1 \\ M_1 \end{Bmatrix} = -\mathbf{K_{11}} \left(\int_0^l n(x) \begin{Bmatrix} b_{u1} \\ 0 \\ 0 \end{Bmatrix} dx + \int_0^l q(x) \begin{Bmatrix} 0 \\ b_{w1} \\ b_{\theta 1} \end{Bmatrix} dx \right) \tag{18}$$

Regarding the fact that the equivalent nodal forces have the same value and the opposite sign of support reactions, by rewriting equations (17) and (18) and separating the axial and flexural deformations, it can be obtained

$$\begin{Bmatrix} F_1 \\ F_4 \end{Bmatrix} = \mathbf{G_a} \int_0^l n(x) \mathbf{b_a} dx \tag{19a}$$

$$\begin{Bmatrix} F_2 \\ F_3 \\ F_5 \\ F_6 \end{Bmatrix} = \mathbf{G_f} \int_0^l q(x) \mathbf{b_f} dx \tag{19b}$$

Where $\mathbf{b_a} = \{b_{u1} \quad b_{u2}\}^T$ and $\mathbf{b_f} = \{b_{w1} \quad b_{\theta 1} \quad b_{w2} \quad b_{\theta 2}\}^T$. $\mathbf{G_a}$ and $\mathbf{G_f}$ are matrices containing the nodal axial and flexural stiffness matrices respectively. $F_i, i = 1,2,...,6$ are the equivalent nodal forces depicted in Figure 4.

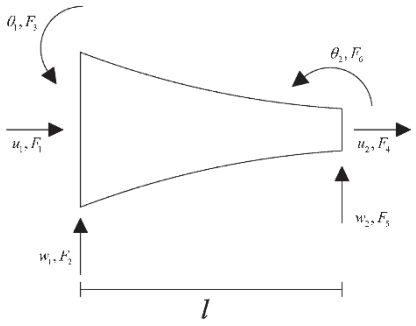

Figure 4. Nodal degrees of freedom and forces (positive sign convention)

$$\mathbf{G_a} = \begin{bmatrix} b_{u1}(0) & 0 \\ 0 & b_{u2}(l) \end{bmatrix}^{-1} \tag{20a}$$

$$\mathbf{G_f} = \begin{bmatrix} b_{w1}(0) & b_{\theta 1}(0) & 0 & 0 \\ \left.\frac{db_{w1}}{dx}\right|_{x=0} & \left.\frac{db_{\theta 1}}{dx}\right|_{x=0} & 0 & 0 \\ 0 & 0 & b_{w2}(l) & b_{\theta 2}(l) \\ 0 & 0 & \left.\frac{db_{w2}}{dx}\right|_{x=l} & \left.\frac{db_{\theta 2}}{dx}\right|_{x=l} \end{bmatrix}^{-1} \tag{20b}$$

5. Strain and kinetic energy formulas

Based on the nonlocal elasticity of Eringen and Euler-Bernoulli beam theory, the strain energy of element could be written as [31]

$$E_U = \frac{1}{2}\int_0^L EI(x)\left(\frac{d^2W}{dx^2}\right)^2 dx + \frac{1}{2}\int_0^L N\left(\frac{dW}{dx}\right)^2 dx + \frac{1}{2}\mu\int_0^L N\left(\frac{d^2W}{dx^2}\right)^2 + \frac{1}{2}\int_0^L EA(x)\left(\frac{dU}{dx}\right)^2 \tag{21}$$

where x is the longitudinal coordinate along beam element, L is the length of beam element, W is the lateral displacement, E and I are the modulus of elasticity and area moment of inertia, respectively.

Furthermore, the kinetic energy of the nanobeam element could be expressed as

$$E_T = \frac{1}{2}\int_0^L \rho A(x)\dot{W}^2 dx + \frac{1}{2}\mu\int_0^L \rho A(x)\left(\frac{d\dot{W}}{dx}\right)^2 dx + \frac{1}{2}\int_0^L \rho A(x)\dot{U}^2 + \frac{1}{2}\mu\int_0^L \rho A(x)\left(\frac{d\dot{U}}{dx}\right)^2 \tag{22}$$

The structural matrices including stiffness matrices ($\mathbf{K_a}, \mathbf{K_f}$), geometric stiffness matrix ($\mathbf{K_g}$) and consistent mass matrices ($\mathbf{M_a}, \mathbf{M_f}$) and the vector of equivalent nodal forces ($\mathbf{F}$) can be written according to FEM

$$\mathbf{K_a} = \int_0^l \mathbf{N_u'}^T EA(x)\mathbf{N_u'} dx \tag{23a}$$

$$\mathbf{K_f} = \int_0^l \mathbf{N_w''}^T EI(x)\mathbf{N_w''} dx \tag{23b}$$

$$\mathbf{K_g} = \int_0^l \mathbf{N_w'}^T P_{cr}\, \mathbf{N_w'} dx + \mu\int_0^l \mathbf{N_w''}^T P_{cr}\, \mathbf{N_w''} dx \tag{23c}$$

$$\mathbf{M_a} = \int_0^l \mathbf{N_u}^T \rho A(x)\mathbf{N_u} dx + \mu\int_0^l \mathbf{N_u'}^T \rho A(x)\mathbf{N_u'} dx \tag{23d}$$

$$\mathbf{M_f} = \int_0^l \mathbf{N_w}^T \rho A(x)\mathbf{N_w} dx + \mu\int_0^l \mathbf{N_w'}^T \rho A(x)\mathbf{N_w'} dx \tag{23e}$$

$$\mathbf{F_a} = \int_0^l n(x)\mathbf{N_u^T} dx \tag{23f}$$

$$\mathbf{F_f} = \int_0^l q(x)\mathbf{N_w^T} dx \tag{23g}$$

in which primes denote differentiation with respect to x; the subscripts **a** and **f** respectively refer to the axial and flexural deformations; $\mathbf{N_w}$ and $\mathbf{N_u}$ are vectors containing shape functions for the lateral and axial deformations respectively.

$$w(x) = \underbrace{\{N_{w1} \quad N_{w2} \quad N_{w3} \quad N_{w4}\}}_{\mathbf{N_w}} \begin{Bmatrix} w_1 \\ \theta_1 \\ w_2 \\ \theta_2 \end{Bmatrix} \tag{24a}$$

$$u(x) = \underbrace{\{N_{u1} \quad N_{u2}\}}_{\mathbf{N_u}} \begin{Bmatrix} u_1 \\ u_2 \end{Bmatrix} \tag{24b}$$

Comparing equation (20a) with equation (23a),

the axial shape functions can be achieved.

$$\mathbf{N_u} = \mathbf{b_a}^T \mathbf{G_a} \tag{25}$$

Similarly, the transverse shape functions are obtained

by comparing equation (20b) with equation (23b).

$$\mathbf{N_w} = \mathbf{b_f}^T \mathbf{G_f} \tag{26}$$

The structural matrices and vectors can be calculated using equations (23).

$$\mathbf{K_a} = \mathbf{G_a}\left(\int_0^l \mathbf{b'_u}^T H(x)\mathbf{b'_u}dx\right)\mathbf{G_a} \tag{27a}$$

$$\mathbf{K_f} = \mathbf{G_f}\left(\int_0^l \mathbf{b''_w}^T D(x)\mathbf{b''_w}dx\right)\mathbf{G_f} \tag{27b}$$

$$\mathbf{K_g} = \mathbf{G_f}\left(\int_0^l \mathbf{b'_w}^T P_{cr}\,\mathbf{b'_w}dx + \mu\int_0^l \mathbf{b''_w}^T P_{cr}\,\mathbf{b''_w}dx\right)\mathbf{G_f} \tag{27c}$$

$$\mathbf{M_a} = \mathbf{G_a}\left(\int_0^l \mathbf{b_u}^T \rho A(x)\mathbf{b_u}dx + \mu\int_0^l \mathbf{b'_u}^T \rho A(x)\mathbf{b'_u}dx\right)\mathbf{G_a} \tag{27d}$$

$$\mathbf{M_f} = \mathbf{G_f}\left(\int_0^l \mathbf{b_w}^T \rho A(x)\mathbf{b_w}dx + \mu\int_0^l \mathbf{b'_w}^T \rho A(x)\mathbf{b'_w}dx\right)\mathbf{G_f} \tag{27e}$$

$$\mathbf{F_a} = \mathbf{G_a}\int_0^l n(x)\mathbf{b_u}^T dx \tag{27f}$$

$$\mathbf{F_f} = \mathbf{G_f}\int_0^l q(x)\mathbf{b_w}^T dx \tag{27g}$$

Owing to the fact that the transverse natural frequency disappears when the axial compressive load reaches its critical value (P_{cr}); in other words, ω_T in equation (4b) is set to zero for instability analysis. Consequently, the following equation can be deduced from equation (4b) for calculation of critical compressive load.

$$\mathbf{K_a^g}\phi = \mu_L^2 \mathbf{M_a^g}\phi \tag{28a}$$

Free transverse vibration

$$\mathbf{K_f^g}\phi = \mu_T^2 \mathbf{M_f^g}\phi \tag{28b}$$

Instability analysis

$$(\mathbf{K_f^g} + \lambda \mathbf{K_g^g})\phi = \mathbf{0} \tag{28c}$$

where μ_L and μ_T are the longitudinal and transverse natural frequencies of the beam, respectively and ϕ is the mode shape vector. The superscript $\mathbf{g}$ is used to denote the global structural matrix obtained by assembling the matrices of all elements and imposing the b μ_T boundary conditions. λ is the eigenvalue of the instability analysis equation and the critical load can be expressed as

6. Structural analysis

Free vibration and instability analyses of nanobeams can be investigated through solving an eigenvalue problem of the following equations

Free longitudinal vibration

$$P_{cr} = \lambda P \tag{28d}$$

where P is the constant compressive load.

7. Numerical examples

7.1. *Free transverse vibration*

In this section, we scrutinize the effect of small scale on the frequency of free transverse vibration of nanobeams through solving a numerical example. Consider a (5,5) armchair SWNT as described in [32] with the following properties: diameter d = 0.678 nm, length L = 10d, effective tube thickness t =0.066 nm, Young's modulus E = 5.5 TPa. Symbols C, S and F represent clamped, simple and free boundary conditions, respectively. The beam is divided to 10 elements in order to solve the problem numerically.

In addition, the six shape functions are presented in Figure 5.

8. Discussion

The first five dimensionless natural frequencies of free transverse vibration of the nanobeam with various boundary conditions for different values of scaling effect parameter are presented in Table 1. Comparing the results with those in the literature, it is observed that the results predicted by the proposed method are in good agreement with the previously published ones though considering just a few elements (10 elements). As illustrated in Figure 6, an increase in scaling effect parameter results in a decrease in the first three natural frequencies of vibration for all various boundary conditions. It is also can be concluded that the effect of the scale parameter intensifies in higher modes. Regarding Table 2 and Figure 7, natural longitudinal frequencies of the nanobeam decreases as the size effect parameter increases and this effect is more significant in higher modes.

7.2. *Free longitudinal vibration*

Considering the nanobeam described in previous section and dividing it to 20 elements, the first three free longitudinal frequencies have been computed and the results have been tabulated in Table 1 and compared with those presented by Aydogdu [40].

7.3. *Instability analysis*

The instability analysis of the axially loaded nanobeam element is presented here. We have assumed E = 1TPa, diameter d=1 nm, and I = πd4/64. The beam has been divided into 10 elements and the results have been compared to those of Wang et al. [41]. Good agreement between the calculated results and those are in the literature has been demonstrated through the Table 3.

Table 1. The first five frequency parameters $\sqrt{\Omega}$ of cantilever and clamped rods, with L/d = 10 for different values of scaling effect parameter $\alpha = e_0 a/L$. (frequency parameter $\Omega^2 = \mu_L^2 \rho L^2/E$)

	α									
	0		0.1		0.3		0.5		0.7	
Mode number	BDF	[40]	BDF	[40]	BDF	[40]	BDF	[40]	BDF	[40]
Clamped beam										
1	1.7727	1.7725	1.7314	1.7312	1.5121	1.5120	1.2989	1.2989	1.1404	1.1404
2	2.5079	2.5066	2.3074	2.3066	1.7162	1.7160	1.3806	1.3805	1.1803	1.1803
3	3.0735	3.0700	2.6205	2.6189	1.773	1.7727	1.3988	1.3987	1.1885	1.1885
Cantilever beam										
1	1.2534	1.2533	1.2457	1.2457	1.1921	1.1920	1.1115	1.1115	1.0281	1.0280
2	2.1714	2.1708	2.0651	2.0647	1.6498	1.6496	1.3569	1.3569	1.1693	1.1692
3	2.8047	2.8025	2.4865	2.4853	1.7519	1.7517	1.3922	1.3922	1.1856	1.1855

Table 1. The first five frequency parameters $\sqrt{\Omega}$ of simply supported, clamped–simply supported, clamped and cantilever beams with $L/d=10$ for different values of scaling effect parameter $\alpha=e_0a/L$. (frequency parameter $\Omega^2=\mu_T^2\rho AL^4/EI$)

Mode number	α = 0		0.1		0.3		0.5		0.7	
	BDF	[32]	BDF	[32]	BDF	[32]	BDF	[32]	BDF	[32]
	Simply supported beam									
1	3.1416	3.1416	3.0685	3.0685	2.6800	2.6800	2.3022	2.3022	2.0212	2.0212
2	6.2832	6.2832	5.7817	5.7817	4.3014	4.3013	3.4604	3.4604	2.9585	2.9585
3	9.4249	9.4248	8.0401	8.0400	5.4423	5.4422	4.2941	4.2941	3.6485	3.6485
4	12.5670	1.566	9.9166	9.9161	6.3633	6.3630	4.9823	4.9820	4.2234	4.2234
5	15.710	15.708	11.5126	11.5111	7.1577	7.1568	5.5832	5.5825	4.7273	4.7273
	Clamped–simply supported beam									
1	3.9266	3.9266	3.8209	3.8209	3.2828	3.2828	2.7899	2.7899	2.4364	2.4364
2	7.0686	7.0686	6.4649	6.4649	4.7668	4.7668	3.8325	3.8325	3.2776	3.2776
3	10.2104	10.2102	8.6519	8.6517	5.8373	5.8371	4.6106	4.6105	3.9202	3.9201
4	13.3527	13.3518	10.4695	10.469	6.7148	6.7143	5.2636	5.2632	4.4648	4.4644
5	16.4960	16.4934	12.0198	12.018	7.4786	7.4773	5.8395	5.8384	4.9473	4.9464
	Clamped beam									
1	4.7300	4.7300	4.5945	4.5945	3.9183	3.9184	3.3153	3.3153	2.8893	2.8893
2	7.8533	7.8532	7.1403	7.1402	5.1964	5.1963	4.1561	4.1561	3.5463	3.5462
3	10.9960	10.9956	9.2586	9.2583	6.2320	6.2317	4.9330	4.9328	4.1998	4.1996
4	14.1384	14.1372	11.0169	11.016	7.0490	7.0482	5.5219	5.5213	4.6822	4.6816
5	17.2820	17.2787	12.5222	12.520	7.7974	7.7955	6.0978	6.0963	5.1703	5.1689
	Cantilever beam									
1	1.8751	1.8751	1.8539	1.8792	1.7155	1.9154	1.5380	2.0219	1.3809	—
2	4.6941	4.6941	4.3745	4.5475	3.3671	3.7665	2.7922	2.9433	2.4404	—
3	7.8548	7.8548	6.8187	7.1459	4.8041	5.2988	3.8520	—	3.2953	—
4	10.9959	10.9955	8.8440	9.2569	5.8415	6.1385	4.6110	—	3.9233	—
5	14.1384	14.1372	10.5749	11.016	6.7205	7.1450	5.2682	—	4.4703	—

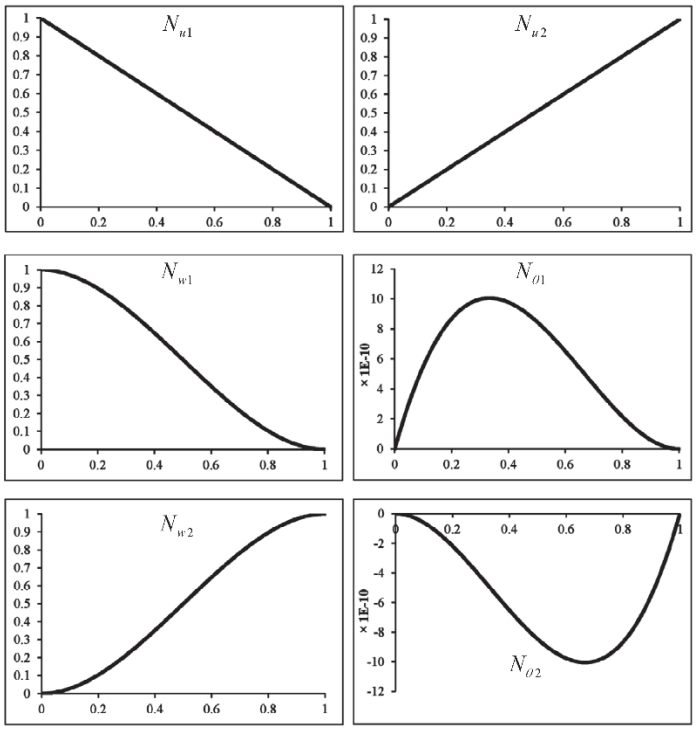

Figure 5. Shape functions of a general nanobeam element

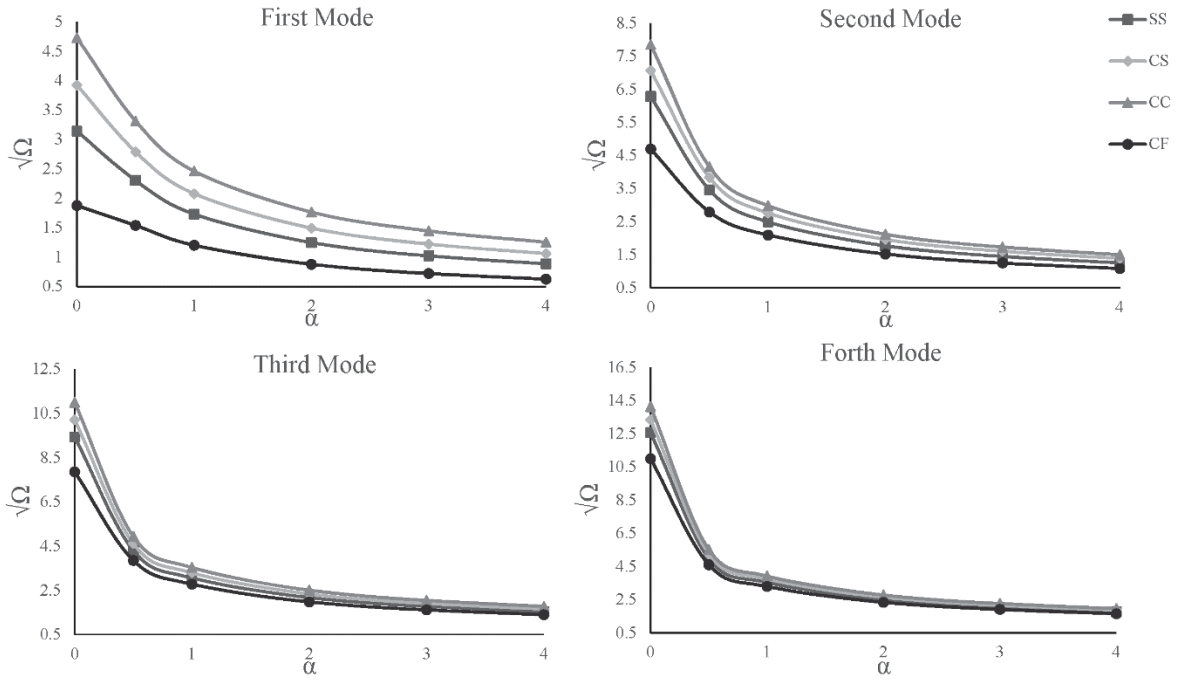

Figure 6. The first four dimensionless natural frequencies of free transverse vibration of the nanobeam for different boundary conditions ($\alpha = e_0 a / l$).

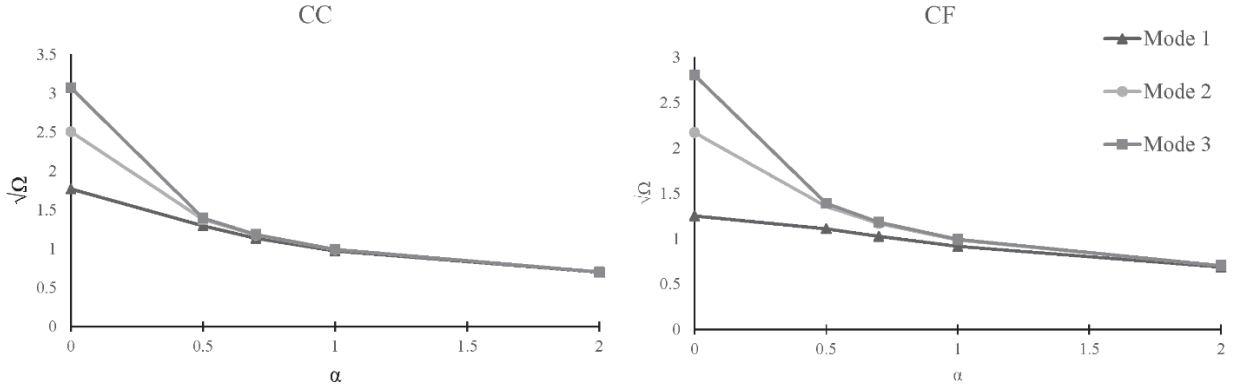

Figure 7. The first three dimensionless natural frequencies of free transverse vibration of the nanobeam for different boundary conditions ($\alpha = e_0 a / l$).

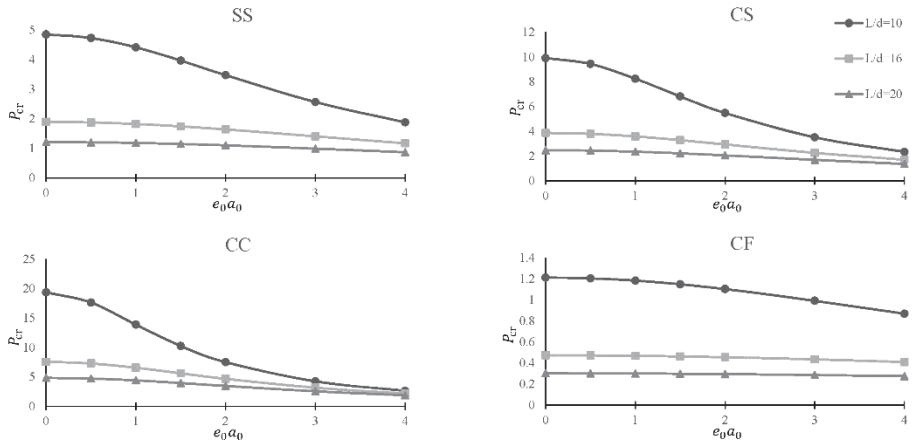

Figure 8. The critical buckling load for different values of L/d and e_0a_0

The critical buckling loads for different values of L/d and are presented In Table 3. As depicted in Figure 8 the scaling effect has a considerable adverse influence on critical buckling load particularly in lower L/d ratios.

$e_0a(nm)$	0		0.5		1		1.5		2	
L/d	BDF	[41]	BDF	[41]	BDF	[41]	BDF	[41]	BDF	[41]
Simply supported beam										
10	4.8447	4.8447	4.7281	4.7281	4.4095	4.4095	3.9644	3.9644	3.4735	3.4735
12	3.3644	3.3644	3.3077	3.3077	3.1486	3.1486	2.9149	2.9149	2.6405	2.6405
14	2.4718	2.4718	2.4411	2.4411	2.3533	2.3533	2.2202	2.2202	2.0574	2.0574
16	1.8925	1.8925	1.8744	1.8744	1.8222	1.8222	1.7414	1.7414	1.6396	1.6396
18	1.4953	1.4953	1.4840	1.4840	1.4511	1.4511	1.3994	1.3993	1.3329	1.3329
20	1.2112	1.2112	1.2038	1.2037	1.1820	1.1820	1.1475	1.1475	1.1024	1.1024
Clamped–simply supported beam										
10	9.9111	9.9155	9.4349	9.4349	8.2461	8.2461	6.8151	6.8151	5.4829	5.4830
12	6.8827	6.8858	6.6496	6.6496	6.0364	6.0363	5.2321	5.2321	4.4096	4.4096
14	5.0567	5.0589	4.9297	4.9297	4.5844	4.5844	4.1052	4.1052	3.5811	3.5811
16	3.8715	3.8715	3.7967	3.7967	3.5885	3.5885	3.2880	3.2880	2.9431	2.9431
18	3.0590	3.0603	3.0121	3.0121	2.8795	2.8795	2.6828	2.6828	2.4486	2.4489
20	2.4778	2.4789	2.4469	2.4469	2.3587	2.3597	2.2251	2.2251	2.0615	2.0615
Clamped beam										
10	19.3791	19.379	17.6383	17.6381	13.8940	13.8939	10.2629	10.263	7.5138	7.5137
12	13.4578	13.458	12.5945	12.5944	10.5621	10.562	8.3234	8.3233	6.4187	6.4187
14	9.8873	9.8872	9.4133	9.4132	8.2297	8.2296	6.8038	6.8038	5.4756	5.4756
16	7.5700	7.5699	7.2890	7.28888	6.5586	6.55849	5.6200	5.6199	4.6819	4.6819
18	5.9812	5.9811	5.8044	5.80434	5.3316	5.33152	4.6943	4.6942	4.0213	4.0212
20	4.8448	4.8447	4.7281	4.72807	4.4096	4.40953	3.9644	3.9644	3.4735	3.4735
Cantilever beam										
10	1.2112	1.2112	1.2038	1.2037	1.1820	1.18202	1.1475	1.1475	1.1024	1.1024
12	0.8411	0.8411	0.8375	0.8375	0.8269	0.8269	0.8099	0.8099	0.7871	0.7871
14	0.6180	0.6179	0.6160	0.6160	0.6103	0.6103	0.6009	0.6009	0.5883	0.5883
16	0.4731	0.4731	0.4720	0.4720	0.4686	0.4686	0.4631	0.4631	0.4556	0.4555
18	0.3738	0.3738	0.3731	0.3731	0.3710	0.3710	0.3675	0.3675	0.3628	0.3628
20	0.3028	0.3028	0.3023	0.3023	0.3009	0.3009	0.2987	0.2986	0.2955	0.2955

Table 3. Critical buckling loads P_{cr} (nN) for simply supported, clamped–simply supported, clamped and cantilever beams with various length-to-diameter ratios L/d and scaling coefficients e_0a .

The six shape functions for free longitudinal and transverse vibration of the nanobeam are derived in terms of BDFs. It is noteworthy that these functions depend on physical and geometrical properties of the nanobeam; however, in this case, due to the constant modulus of elasticity, cross section, mass density and moment of inertia they are apparently independent. e_0a_0

The first four mode shapes of transverse vibration of the nanobeam are depicted in Figure 9 for different values of the scaling effect parameter. It is observed

that the size effect influences on mode shapes especially in higher vibration modes.

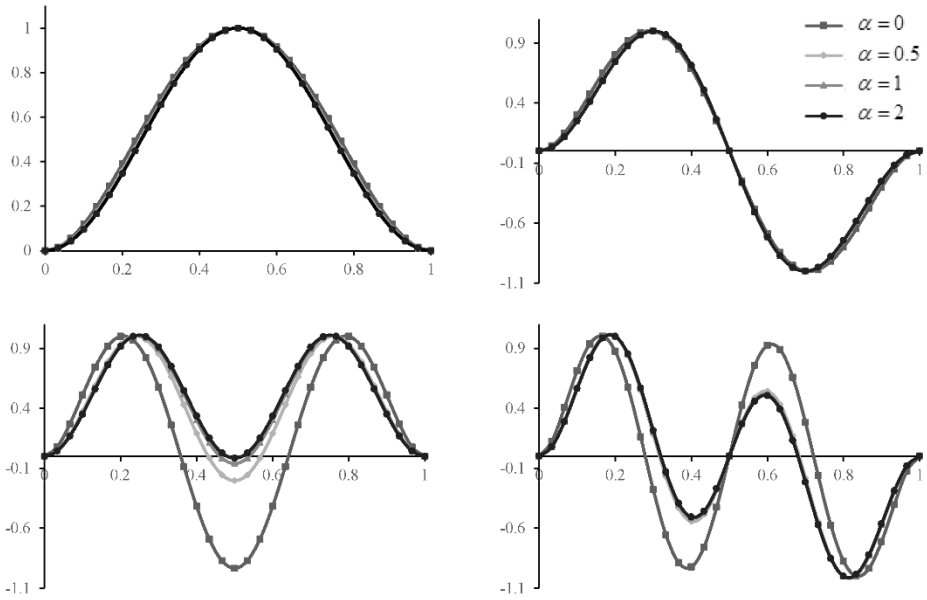

Figure 9. The first four normalized mode shapes of nanobeams described in the examples

9. Conclusions

In this article, the innovative basic displacements functions were introduced, developed and exploited for structural analysis of nanobeams employing Eringen's nonlocal elasticity and Euler-Bernoulli beam theory. The flexibility basis of the proposed method inherently satisfies the equilibrium equations at each inner point of the element. The efficiency and accuracy of the proposed method for the above mentioned boundary conditions in stability analysis, free longitudinal vibration and free transverse vibration were demonstrated through several numerical examples. Convergence of the result was achieved by exploiting just 10 of the proposed elements in the finite element procedure []. According to the attained results, it is concluded that the size effect plays an important role in stability analysis, free longitudinal vibration and free transverse vibration of nanobeam.

References

1. Postma H.W.C., Teepen T., Yao Z., Grifoni M., Dekker C., 2001, Carbon nanotube single- electron transistor at room temperature, Science **293**: 76-79.

2. Kim C., Zhang S., 2009, Conductivity of carbon nanofiber/polypyrrole conducting nanocomposites, J Mech Sci Technol **23**: 75-80.

3. Hall A.R., Falvo M.R., 2006, Superfine R and Washburn S. Electromechanical response of single-walled carbon nanotubes to torsional strain in a self-contained device, Nature **2:** 413-416.

4. Kis A., Kasas S., Babic B., Kulik A.J., Benoit W., Briggs G.A.D., Schonenberger C., Catsicsa S., Forro L., 2002, Nanomechanics of Microtubules, Phys Rev Lett **89:** 248101.

5. Cuenot S., Fretigny C., Demoustier-Champagne S., Nysten B., 2003, Measurement of elastic modulus of nanotubes by resonant contact atomic force microscopy, J Appl Phys **93:** 5650.

6. Juhasz J.A., Best S.M., Brooks R., Kawashita M., Miyata N., Kokubo T., Nakamura T., Bonfield W., 2004, Mechanical properties of glass-ceramic A–W-polyethylene composites: effect of filler content and particle size, Biomaterials **25:** 949-955.

7. Sorop T.G., de Jongh L.J., 2007, Size-dependent anisotropic diamagnetic screening in superconducting Sn nanowires, Phys Rev B **75:** 014510.

8. Ghoniem N.M., Busso E.P., Kioussis N., Huang H., 2003, Multiscale modelling of nanomechanics and micromechanics: an overview, Philos Mag **83:** 3475.

9. Eringen A.C., 1972, Nonlocal polar elastic continua, Int J Eng Sci **10:** 1–16.

10. Eringen A.C., and Edelen D., 1972, On nonlocal elasticity, Int J Eng Sci **10:** 233–248.

11. Eringen A.C., 1983, On differential equations of nonlocal elasticity and solutions of screw dislocation and surface waves, J Appl Phys **54:** 4703–4710.

12. Eringen A.C., 2002, Nonlocal continuum field theories, New York: Springer-Verlag.

13. Peddieson J., Buchanan G.R., McNitt R.P., 2003, Application of nonlocal continuum models to nanotechnology, Int J Eng Sci **41:** 305–312.

14. Sudak L.J., 2003, Column buckling of multiwalled carbon nanotubes using nonlocal continuum mechanics, J Appl Phys **94:** 72-81.

15. Polizzotto C., Fuschi P., Pisano A.A., 2006, A nonhomogeneous nonlocal elasticity model, Eur J Mech A Solids **25:** 308–333.

16. Pisano A.A., Sofi A., Fuschi P., 2009, Finite element solutions for nonhomogeneous nonlocal elastic problems, Mech Res Commun **36:** 755–761.

17. Paola M.D., Pirrotta A., Zingales M., 2010, Mechanically-based approach to non-local elasticity: variational principles, Int J Solids Struct **47:** 539–548.

18. Mahmoud F.F., Meletis E.I., 2010, Nonlocal finite element modeling of the tribological behavior of nano-structured materials, Interact Multiscale Mech **3:** 267–276.

19. Phadikar J.K., Pradhan S.C., 2010, Variational formulation and finite element analysis for nonlocal elastic nanobeams and nanoplates, Comput Mater Sci **49:** 492–499.

20. Lim C.W., 2010, On the truth of nanoscale for nanobeams based on nonlocal elastic stress field theory: equilibrium, governing equation and static deflection, Appl Math Mech **31:** 37–54.

21. Rafiei M., Mohebpour S.R., Daneshmand F., 2012, Small-scale effect on the vibration of non-uniform carbon nanotubes conveying fluid and embedded in viscoelastic medium, Phys E **44:** 1372–1379.

22. Eltaher M.A., Emam S.A, Mahmoud F.F., 2012, Free vibration analysis of functionally graded size-dependent nanobeams, Appl Math Comput **218:** 7406–7420.

23. Mahmoud F.F., Eltaher M.A., Alshorbagy A.E., Meletis E.I., 2012, Static analysis of nanobeams including surface effects by nonlocal finite element, J Mech Sci Tech **26:** 1–9.

24. Wang Q., C M Wang C.M., 2007, The constitutive relation and small scale parameter of nonlocal continuum mechanics for modelling carbon nanotubes, Nanotechnology **18(7):** 075702.

25. Danesh M., Farajpour A., Mohammadi M., 2012, Axial vibration analysis of a tapered nanorod based on nonlocal elasticity theory and differential quadrature method, Mech. Res. Comm. **39**: 23–27.

26. Aghababaeia R, Reddy, J.N., 2009, Nonlocal third-order shear deformation plate theory with application to bending and vibration of plates, J. Sound Vib., Vol. **326:** 277–289.

27. Farajpoura A., Mohammadia M., Shahidia A.R., Mahzoonb M., 2011, Axisymmetric buckling of the circular graphene sheets with the nonlocal continuum plate model, Physica E, **43(10):** 1820-1825.

28. McFarland A.W., and Colton J.S., 2005, Role of material microstructure in plate stiffness with relevance to microcantilever sensors, J Micromech Microeng **15:** 1060–1067.

29. Wang Q., Liew K.M., 2007, Application of nonlocal continuum mechanics to static analysis of micro- and nano-structures, Phys Lett A **363:** 236–242.

30. Xu M., 2006, Free transverse vibrations of nano-to-micron scale beams, Proc Roy Soc A **462:** 2977–2995.

31. Reddy J.N., 2007, Nonlocal theories for bending, buckling and vibration of beams, Int J Eng Sci **45:** 288–307.

32. Wang C.M., Zhang Y.Y., He X.Q., 2007, Vibration of nonlocal Timoshenko beams, Nanotechnology **18:** 105401.

33. Heireche H., Tousi A., Benzair A., Maachou M., Bedia E.A., 2008, Sound wave propagation in single-walled carbon nanotubes using nonlocal elasticity. Phys E **40:** 2791–2799.

34. Aydogu M., 2009 A general nonlocal beam theory: its application to nanobeam bending, buckling and vibration. Phys E **41:** 1651–1655.

35. Kong S., Zhou S., Nie Z., wang K., 2008, The size-dependent natural frequency of Bernoulli–Euler micro-beams, Int J Eng Sci **46:** 427–437.

36. Kong S., Zhou S., Nie Z., wang K., 2009, Static and dynamic analysis of micro beams based on strain gradient elasticity theory, Int J Eng Sci **47:** 487–498.

37. Filiz S., Aydogu M., 2010, Axial vibration of carbon nanotube heterojunctions using nonlocal elasticity, Comput Mater Sci **49:** 619–627.

38. Xia W., Wang L., Yin L., 2010, Nonlinear non-classical microscale beams: static bending, postbuckling and free vibration, Int J Eng Sci **48:** 2044–2053.

39. Wang B.L., Hoffman M., Yu A.B.m 2012, Buckling analysis of embedded nanotubes using gradient continuum theory, Mech Mater **45:** 52–60.

40. Aydogdu M., 2009, Axial vibration of the nanorods with the nonlocal continuum rod model, Physica E **41:** 861–864.

41. Wang C.M., Zhang Y.Y., Ramesh S.S., Kitipornchai S., 2006, Buckling analysis of micro- and nano-rods/tubes based on nonlocal Timoshenko beam theory, J Phys D: Appl Phys **39:** 3904–3909.

42. Attarnejad R., 2010, Basic displacement functions in analysis of nonprismatic beams, Eng Comput **27:** 733-745.

43. Shahba A., Attarnejad R., Hajilar S., 2013, A Mechanical-Based Solution for Axially Functionally Graded Tapered Euler-Bernoulli Beams, Mech Adv Mater Struc **20:** 696–707.

44. Attarnejad R., Shahba A., 2011, Basic Displacement Functions in Analysis of Centrifugally Stiffened Tapered Beams, Arab J Sci Eng **36:** 841–853.

45. Attarnejad R., Shahba A., Jandaghi Semnani S., 2011, Analysis of Non-Prismatic Timoshenko Beams Using Basic Displacement Functions, Adv Struct Eng **14:** 319-332.

46. Attarnejad R., Shahba A., Eslaminia M., 2011, Dynamic basic displacement functions for free vibration analysis of tapered beams, JVC **17:** 1–17.

47. Attarnejad R., Shahba A., 2011, Dynamic basic displacement functions in free vibration analysis of centrifugally stiffened tapered beams; a mechanical solution, Meccanica **46:** 1267-1281.

48. Attarnejad R., Jandaghi Semnani S., Shahba A., 2010, Basic displacement functions for free vibration analysis of non-prismatic Timoshenko beams, Finite Elem Anal Des **46:** 916–929.

49. Shahba A., Attarnejad R., Jandaghi Semnani S., Shahriari V., Dormohammadi A.A., 2012, Derivation of an efficient element for free vibration analysis of rotating tapered Timoshenko beams using basic displacement functions, P I Mech Eng G-J Aer **226:(11)** 1455-1469.

50. Qaisi M.I., 1996, A power series approach for the study of periodic motion, JSV 196(4):401–406.

51. Bhaskar K, Dhaoya J., 2009, Straightforward power series solutions for rectangular plates, Compos Struct **89:** 253–61.

52. A. Farajpoura A., Shahidia A.R., Mohammadia M., 2012, Buckling of orthotropic micro/nanoscale plates under linearly varying in-plane load via nonlocal continuum mechanics, Compos Struct **94:** 1605–1615.